Construction and Building Materials 199 (2019) 637–651

Contents lists available at ScienceDirect

Construction and Building Materials

journal homepage: www.elsevier.com/locate/conbuildmat

Review

A review of X-ray computed tomography of concrete and asphalt construction materials

Anton du Plessis [a,b,*], William P. Boshoff [c]

[a] Stellenbosch University CT Facility, Stellenbosch University, South Africa
[b] Physics Department, Stellenbosch University, South Africa
[c] Department of Civil Engineering, Stellenbosch University, South Africa

HIGHLIGHTS

- The use of X-ray microCT for concrete and asphalt building materials is reviewed.
- Successful applications of this technique to concrete and asphalt materials are summarized.
- Insight into the current capabilities and state of the art is provided.
- Newly developed methods are discussed and demonstrated.
- Suggestions are made for sampling and scan strategies for different analysis types.

ARTICLE INFO

Article history:
Received 17 May 2018
Received in revised form 8 October 2018
Accepted 11 December 2018
Available online 19 December 2018

Keywords:
Computed tomography
microCT
Cement-based materials
Concrete
Asphalt
Non-destructive testing

ABSTRACT

The microstructural details of concrete and asphalt construction materials are crucial in understanding and improving their material properties for structural applications in civil engineering. Various destructive and non-destructive test methods are widely used in this field, but the use of non-destructive X-ray micro computed tomography is still widely under-estimated and the capabilities not yet fully appreciated. This review summarises the successful applications of this technique to concrete and asphalt materials to date and thereby provides insight into the current capabilities and state of the art. The review is structured according to the different types of analyses possible, and include examples of each, which helps to demonstrate the potential of the technique as applied to these types of structural materials. The recent growth in the use of the technique is related to its increased accessibility and newly developed methods which are discussed and demonstrated. Suggestions are made for sampling and scan strategies for the different analysis types.

Contents

* Corresponding author at: Stellenbosch University CT Facility, Stellenbosch University, South Africa.
E-mail address: anton2@sun.ac.za (A. du Plessis).

https://doi.org/10.1016/j.conbuildmat.2018.12.049
0950-0618/

1. Introduction

1.1. Background

X-ray computed tomography (CT) and micro computed tomography (microCT) has been used for non-medical materials analysis for a number of years, with the last 10 years seeing the technique evolve from a qualitative imaging tool to a quantitative analysis method, in materials science in particular [1]. The method has also found particular application in geomaterials and geosciences as has been discussed in the review paper [2]. Other fields were the technique is well established is for industrial non-destructive testing applications [3], dimensional metrology [4], additive manufacturing [5], food science [6] and biological sciences [7]. The recent growth and development of the technique has been driven by advances in equipment hardware availability and the development of software tools for the analysis and handling of the large data sets generated. Despite the tremendous growth, there has not been a thorough review of the applications relevant to concrete and asphalt construction materials. There has been only one book chapter summarising the use of the technique in civil engineering in general [8]. The present review article aims to fill this gap and demonstrate the current state of the art.

1.2. Historical perspective

In the early days of X-ray microCT, the 3D characterization of aggregates and the void distribution in asphalt was already considered useful as outlined in [9–11]. Earlier studies were focused on visualisation and image segmentation, or indicating the ability to non-destructively visualize the internal details of concretes and other cement based materials [12–14]. Prior to the availability of high resolution microCT, there have been various efforts using medical X-Ray CT scanners with reasonably good results despite the poor resolution relative to microCT – the increased X-ray intensity results in sharper images and better contrast for large features, as demonstrated in a direct comparison for a concrete block in [15]. The terms CT and microCT are often used interchangeably, but generally both techniques use X-ray radiation and CT is typically referred to when scans are done using medical scanners with resolutions of approximately 0.5 mm, while microCT typically refers to laboratory cone beam scanners where resolutions are variable from 0.3 mm down to typically 0.005 mm (5 μm) or lower.

The early works where the high resolution microCT technique was applied to concrete and asphalt materials were reviewed in 2008 [16]. Although there had been numerous studies making use of X-ray microCT to image concrete and asphalt materials earlier than 2008, the true potential of the technique has only in the last 10 years become apparent, as the quantitative analysis capabilities have been developed further, and these have been utilised beyond the point of demonstration only – ie. to answer specific and often very interesting scientific questions relevant to these materials.

Almost 10 years ago, Cnudde et al [17] demonstrated the huge potential for microCT of building stones and concretes, showing how 3D visualization and analysis of the porosity in these materials correlate well with traditional measures such as mercury porosimetry, and how this can in some instances provide superior information helping to provide an improved understanding of such building materials. These authors at the time mentioned the general need for improvements in microCT resolution, signal-to-noise ratio and more powerful software in order to bring the technique to its full potential. The last 10 years has seen significant growth and development in exactly these areas, with improvements in computer hardware and software allowing more complex image-based analysis to be performed, while microCT hardware has improved significantly and such systems have also become more widely available.

Numerous studies were published in this last ten years using microCT to analyse concrete and asphalt: these studies can usually be categorized by the type of information gained by microCT, with broad categories being the sections in this review: porosity, phase identification and density, damage and failure analysis, fibre reinforcement, temporal evolution or time-lapse studies (also in-situ studies) and image based simulations and modelling using microCT data. These studies generally either use simple qualitative 3D visualization or quantitative 3D analyses which can sometimes be more complex and time consuming, and are often customized to the application. Qualitative 3D visualizations may be useful for viewing the directionality or clustering of reinforcement fibres, viewing pore shapes or the connectivity of pore networks or for viewing the location and extent of a crack. Quantification of the data in 3D is always necessary when comparing samples, looking for small but important differences between samples or for making quantitative conclusions. Examples of this include total pore fraction, largest pore size, pore size distributions, pore shape distributions, fibre distribution, crack widths, volume fractions of aggregate stones or bitumen and more recently, 3D image-based simulations allowing determination of absolute permeability and maximum flow rates, for given input parameters. Connected porosity can be analysed for flow path complexity using tortuosity analysis of the pore networks. Finally, structural mechanics simulations allow the analysis of stress distributions and effective elastic modulus of the real material, compared to idealized models.

In general not all the above-mentioned information can be obtained from every sample type, and microCT can be applied in different ways, depending on the analysis requirements. Despite the non-destructive nature of the method, some sample preparation may be required to obtain best results for a particular application. For example, for asphalt, an approximately 70 mm core provides a good field of view while maintaining sufficient resolution to visualize the macroporosity and pore network. For its microporosity, an even smaller sample needs to be sectioned, which might require sampling statistically relevant numbers of small sections for microporosity.

This review covers published work mainly in the last 10 years, focusing on the microCT methodologies and strategies that have been used successfully for concrete and asphalt materials in recent years. This demonstrates the type of information that can be acquired and the complexity required for this type of analysis, for concrete and asphalt materials. This provides insight into the current practical capabilities of the technique, also using selected examples from the authors' laboratory. These examples are mostly from as-yet unpublished works. Finally, suggestions are made

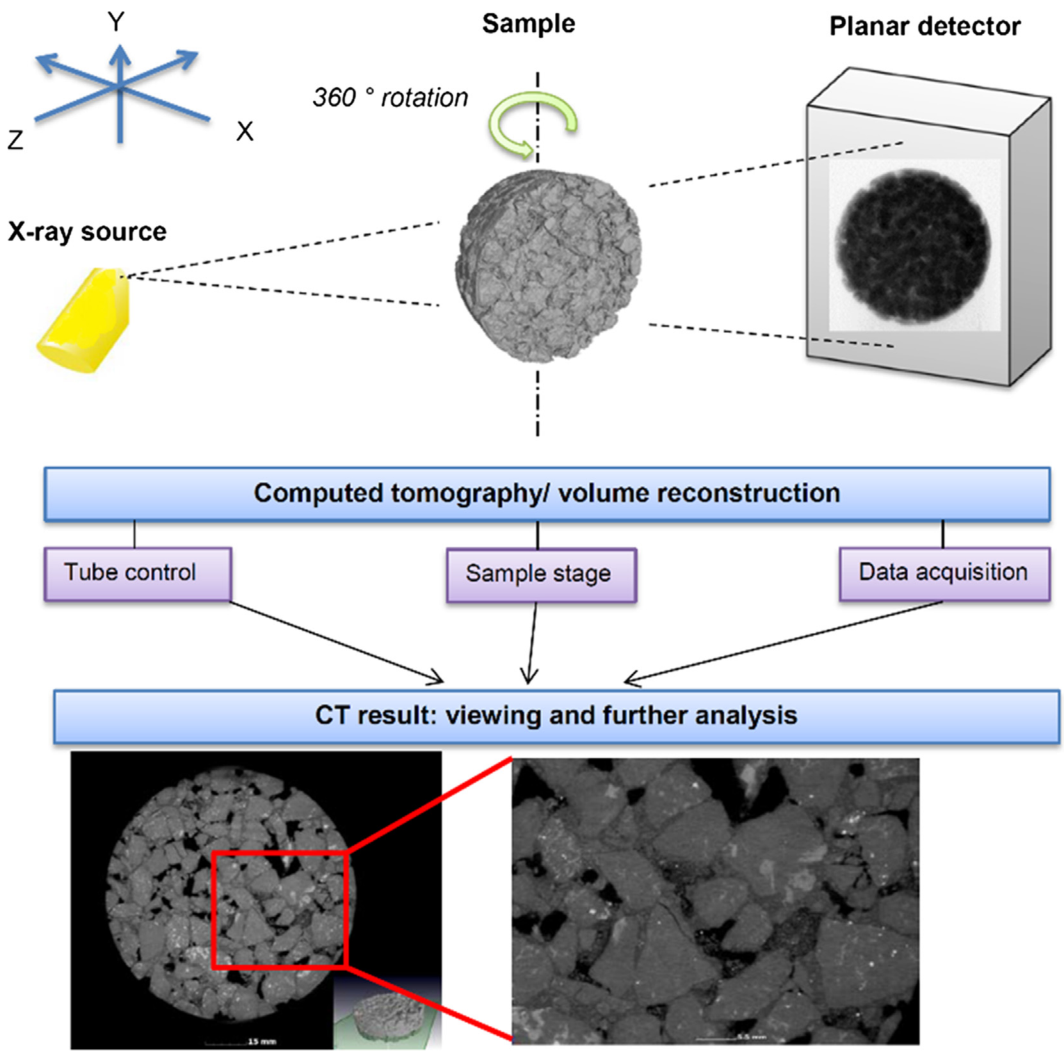

Fig. 1. Schematic of the microCT scan process, as applied to an asphalt sample. The 2D projection images are recorded as the sample is rotated, and shown below is an example of a CT slice image which can be viewed and analysed after reconstruction.

based on the above-mentioned literature and experience for microCT sampling, scanning and image analysis strategies for different types of analysis requirements for concrete and asphalt based materials. All discussions are relevant to both concrete and asphalt materials, and the two material types are used interchangeably in the scope of this review paper.

2. Basic principles of X-ray microCT

X-ray microCT is based on the same principles as medical computerised axial tomography developed originally in the early 1970s for medical imaging [18]. The specialized field of industrial microCT developed in the early 1990s when high resolution X-ray sources and detectors became available allowing high resolution CT in the microscale (medical scanners typically have 0.5 mm or more pixel sizes). The principles of the technique are described in detail in [19], in this section a brief overview is provided.

A typical laboratory microCT system is schematically illustrated in Fig. 1: comprising of an X-ray source, rotation stage with sample, and planar detector. A sample is loaded onto the rotation stage in ambient conditions using low-density mounting materials – usually no further sample preparation is necessary. The sample size and loading angle determines the resolution that can be obtained, hence sample sectioning may be required for the best scan quality and resolution. The cone beam of X-rays is projected onto the sample, creating a 2D projection image on the detector. In this case the disk-shaped sample is loaded in a side-ways configuration to allow least material penetration distance along many angles, allowing a higher contrast. The sample can be loaded at any angle, but keeping flat surfaces angles relative to the X-ray beam direction minimizes surface artifacts. This "real-time" digital X-ray image can often be used for non-destructive testing purposes: major cracks or flaws can be easily identified. X-ray and scan settings are selected based on the sample type and size, and the optimised parameters may vary depending on the goal of the scan, varying the scan time from a few minutes to many hours; a typical good quality scan time is 1 h per sample. For more considerations of scan parameter optimization the reader is referred to [7]. It is important to realize that X-rays are entirely non-destructive and no changes are induced in the sample due to the X-rays, due to the very low doses and low absorption. In the process of CT scanning, the sample is rotated and many (typically between 500 and 4000) 2D projection images are recorded during a full 360 degree rotation. After scanning, these images are used to compute (reconstruct) the volumetric dataset representing the sample. This reconstruction process is typically based on the Feldkamp back-projection algorithm, usually performed with software provided with the hardware [20]. The reconstructed data comprises of a 3D grid of volumetric pixels (voxels) with brightness values related to the X-ray density of the material it represents. X-ray density is related to both physical density and atomic mass, therefore a denser object will appear brighter in the CT data. The asphalt sample in Fig. 1 shows a CT slice image with a close-up region indicating the clear imaging of aggregates, void spaces and bitumen. This is a typical result from CT and requires no further effort for viewing, besides moving slice by slice through the data to view different parts of the sample. This qualitative result (visualization of slices) is often enough, and is cost effective as no further data processing is required.

For further quantitative analysis, various software tools can be used for making different volumetric measurements as are described later in this review. This image analysis procedure is not always obvious and custom analysis procedures sometimes need to be developed for a particular application or sample type. The time investment in image analysis is often under-estimated and remains one of the challenges with CT. All image analysis and processing shown as examples in this review were done using the software Volume Graphics VGSTUDIO MAX 3.2.

The basic microCT process therefore involves the sample setup, scanning, reconstruction and image visualization and analysis. Basic guidelines for microCT scanning can be found in [7], which are aimed at biological samples, but generally the guidelines are similar for all material types. Concrete materials are denser and might contain heavier atomic compositions than typical biological samples, so higher voltages and beam filtration is typically required. This makes beam hardening correction very important as well, in order to obtain useful images. Beam hardening refers to increased absorption of lower-energy X-rays as the beam moves through a sample, resulting in inhomogenous attenuation of the beam energies in different materials and along different path lengths in the sample. The result is brighter areas near the edges of the sample compared to the interior (cupping effect) and in extreme cases streaks around dense objects (streak effects). Most of the work presented in this review can be done at a typical laboratory microCT facility such as that described in [21]. Besides these typical systems, other variations are accessible. These include in particular: (a) higher voltage micro/macroCT systems up to 600 kV for highly dense and large samples, (b) nanoCT systems with voxel sizes down to 50 nm for very high resolution imaging of field of view of 150 μm inside a small sample, and (c) synchrotron tomography which allows any of the above: high resolution, high penetrating ability and fast scanning – this allows advanced applications such as in situ monitoring of changes during loading, for example. The advantage of laboratory-based systems are that they are relatively easier to access and larger sample throughput is typically possible.

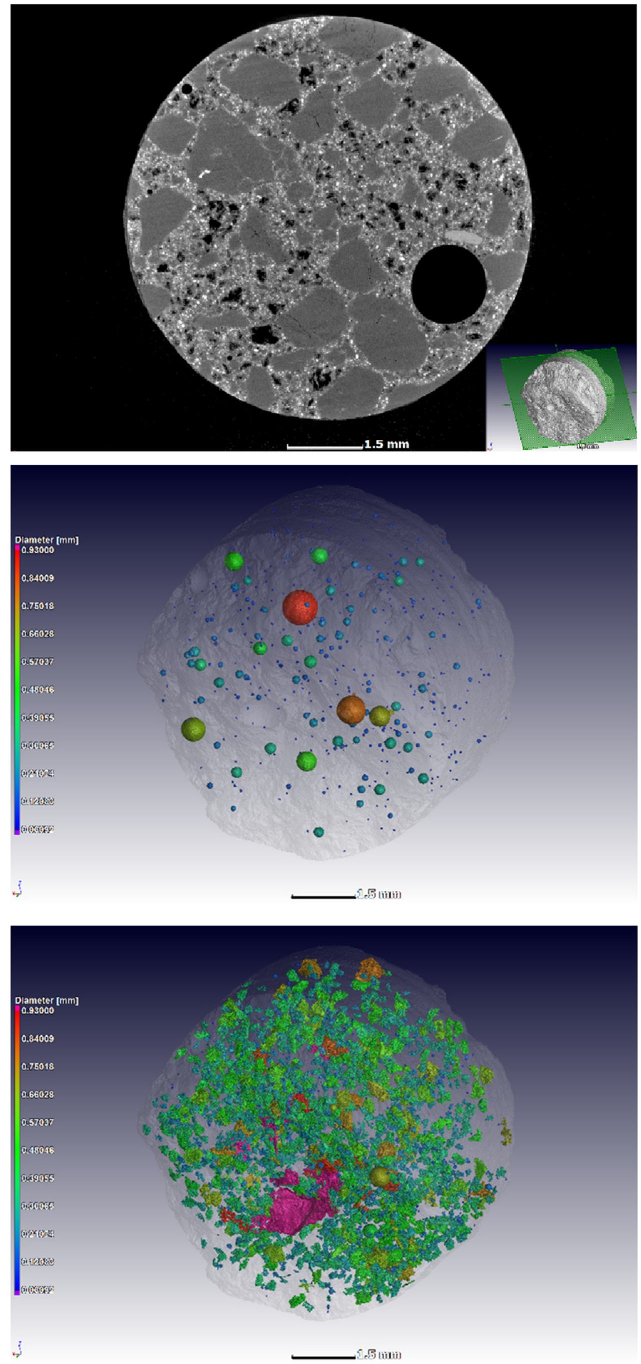

Fig. 2. Porosity analysis of a concrete sample showing (a) CT slice image, (b) porosity analysis of largest spherical pores, (c) porosity analysis of the largest non-spherical pores.

3. Capabilities and analysis methods

3.1. Porosity

One of the most popular applications of microCT is porosity analysis – this refers to the identification of pore spaces or voids in the material, qualitatively visualizing this porosity spatial distribution and quantitatively analyzing it. Qualitatively viewing porosity in 2D slice images is simple and requires only basic image contrasting and scrolling through images from one side of the sample to the other. Quantitative analysis requires the selection of pore spaces by image segmentation, typically using some form of thresholding to delineate the edge between pore space and material. Once the segmentation is done, quantitative analysis allows the measurement of volume, surface area, sphericity and other parameters for each void space and analyzing this pore statistical information.

Fig. 2 demonstrates a simplified method of porosity analysis in a small concrete sample with a roughly disk-shaped geometry and diameter of 8 mm. The Fig. 2(a) shows a CT slice image in greyscale, with a large spherical pore shown in the bottom right of the sample, and various smaller irregular shaped pores (black). Also clear are the aggregate (dark grey) and hardened cement paste (brighter grey with variations in intensity, due to chemical or physical density changes). Fig. 2(b) shows the result of a porosity analysis where the selection of pores was limited to those pores having sphericity >0.6 and diameter >60 μm (in other words all the largest, most spherical pores), colour coded according to diameter. Fig. 2(c) shows the result of a porosity analysis where only the pores with sphericity <0.6 were selected in the same sample and colour coded.

The results in Fig. 2 are only visual representations, with a vast amount of additional information that can be extracted: each pore space has values for its total volume, surface area, sphericity, location relative to the surface, XYZ position, projected area in all three axes, etc. Statistical analyses such as pore size distribution can therefore be calculated with this data.

As can be expected, the microCT-based porosity analysis of concrete materials is popular, due to the inherent porosity of these type of materials and the important role these pores can play in their mechanical and transport properties. There are important correlations between pore size distributions and the strength of concrete [22] and the transport properties of concrete [23].

As demonstrated in [17], the pore size distribution in concrete can be quantified and evaluated using X-ray microCT within the range of resolution allowed by the technique. In this study, mercury intrusion porosimetry (MIP) was applied to the same samples subjected to microCT scans and porosity information from this technique compared to that of microCT. It was shown that MIP allows the quantification of pore size distributions smaller than that possible by microCT, but this method can be subject to some errors such as the ink-bottle effect (where many pore connections are small resulting in increased pore size contribution from small pores and an underestimate of larger pore spaces). In this study samples were also scanned after mercury intrusion, highlighting areas of increased porosity including the interfacial transition zone between cement paste and aggregate, which was not visible in scans prior to mercury intrusion. It was also noticed that a crack appeared in an aggregate which may possibly be attributed to the mercury intrusion process.

Often porosity is measured by 2D sectioning [24] and image analysis: this is called stereology [25]. In a study by Kim et al [26], microCT slice images were used for this stereological process. The virtual slicing by microCT eliminated sectioning errors and allowed a comparison of stereological and direct 3D measurements. They found significant inhomogeneity in porosity between slices, which results in the requirement that at least ten 2D slice images are required to provide acceptable average results from the stereological method.

The pore spacing is an important factor affecting the durability of cement and concrete materials subjected to freeze-thaw cycles, therefore special 3D measures of the pore spacing were devised in [27]. It was shown that the method works well but it was mentioned that high resolution and small sample sizes are required, making it difficult to apply when large aggregates are used. In a recent study by [28] small 6 mm concrete cores were analysed for porosity and pore spacing, relevant to freeze-thaw durability of the concrete. Difficulties with image segmentation were discussed in some detail with suggestions made on this process. It was found that the pore spacing factor and specific surface could be reliably calculated, but the sample size limited the ability to determine bulk air content accurately. Damage due to freeze thaw cycles are discussed further in Section 3.3.

Appropriate sampling of the data in the microCT scan is required, as shown in a study of the porosity of small mortar specimens [29]. This work showed deviations between the results obtained by pycnometry and microCT, as one would expect – the gas-based pycnometry method is expected to detect much smaller pore spaces. More interesting is that, as the concrete was dried over 28 days a reduced porosity was observed on the interior but not as pronounced reduction near the surface of the samples. This highlights the need for good selection of regions of interest for analysis, and good sampling strategies required (eg. sample size relative to pore sizes expected). It also demonstrates the additional information obtained by microCT with regard to 3D distribution of features.

Another more recent in-depth study [30] investigated the void system of lightweight concrete, discriminating between voids in the cement paste and those in the aggregate, requiring a custom image analysis procedure. The authors used scans at two resolutions to provide a more thorough combined pore size distribution, using a power law to combine results from the two scans at different scales. The authors mentioned the capability of submicron or nanoCT systems to provide even higher resolution information of smaller pores, such as those trapped inside hollow glass spheres.

High resolution pore analysis was performed in leached cements using microCT and nanoCT instruments at voxel sizes of 1.8 μm and 64 nm, with small field of views (and hence small sample sizes as well) [31]. This allowed the visualisation of pore connectivity and variations in the porosity from different locations relative to the surface.

Porosity in the interface zone between an existing concrete substrate and a new overlay was investigated in [32]. It was shown that the porosity varies in this zone depending on the surface preparation and on the hardening time. The same authors subsequently analysed the pull-off adhesion relative to the porosity in this interface zone [33].

Gas bubble size distributions in foamed cement were analyzed in [34] as a function of foaming parameters. Chung et al [35] analyzed foamed concrete of varying densities – the pore size distributions and more complex measurements including anisotropy of pores were analysed and compared to numerical and experimental results of thermal conductivity and strength. In this case custom image-based analysis procedures were developed using Matlab.

As mentioned before, image analysis can be the limiting step for comparative analysis as this process often depends on the selection of a user-defined threshold value. In the work presented in [36], a simplified image analysis procedure is demonstrated which uses a simple global threshold value, but automatically refines this threshold locally at every point on the interface between the two materials being segmented. This is a relatively simple procedure, available in commercial software, not affected by human choice within a reasonable range. The automatic local optimisation of the threshold is described in more detail in a different study of the quantification of mineral inclusions in rock drill core, where the results where found to be in excellent agreement with traditional mineral quantification methods [37]. Besides the simpler image analysis procedure, strategies for faster scanning was also demonstrated in [36], making the technique more cost effective and therefore more easily accessible. In addition to fast scanning, the scaling of resources through a multi-user microCT facility such as in [21] makes it possible for easier access and lower cost availability of this technology. Scanning multiple samples at once is also possible with reduced quality as discussed in more detail in the next section and in [38].

The above-mentioned simplified image analysis procedure was used in a study of the porosity in high performance concrete made using super-absorbent polymers (SAP) [39], where it was found that the SAP particles increase the total porosity. However this increase was not considered problematic as the SAP pores reduce in size with aging, being partially filled with cementitious products. In different studies of concrete samples containing SAP, microCT was also used with great success to quantify porosity [40,41]. Porosity was also determined effectively by [42] by using a Dual Energy X-Ray microCT method, which allows for improved discrimination between materials of similar density. Besides lab-based microCT, synchrotron CT has also been widely used for characterisation of concrete porosity, see for example [43] where the influence of nano-SiO_2 on the structure of alkali activated slag cement composites was investigated. In a study by [44], the deterioration of the pore network was studied due to electrochemical leaching in the cement.

Despite all the above-mentioned studies of porosity of concrete using microCT, the main limitation for accurate characterization of concrete porosity is the wide range of pore sizes present in such materials, and the limitation of typical laboratory microCT systems in terms of resolution ranges. As mentioned above, nanoscale porosity cannot be measured with the technique, only micro and macro porosity can be measured. A second limitation associated with this is the sample size scaling with achievable resolution – for best quality characterization of small micropores, small sample sizes are needed (eg. 10 mm or smaller) which can lead to loss of macropore information or sampling problems. The scan strategy and resolution therefore is crucial in best making use of the technique for porosity characterization.

It is envisaged that porosity analysis remains one of the major functional uses of microCT of concretes and asphalt materials, with new image analysis procedures allowing increasingly detailed analyses of relative pore spacing, pore distances from the surface or interfacial zones between materials, and local pore concentrations. All these advanced image analysis methods will allow improved understanding of these materials and the role of porosity in their mechanical and other properties.

3.2. Phase identification & density

Phase identification refers to the ability to identify different compositions or components in the microCT images. This is relatively simple when the constituents are known, but requires image segmentation to accurately delineate the materials and assign them. It is important to realize that typical microCT does not allow chemical analysis and the brightness differences between materials are based only on a combination of atomic mass and physical density [19]. Hence two materials might have similar grey values, despite chemical differences. Nevertheless in practice, using high quality scan parameters and good resolution allows the differentiation of most materials from one another. Segmentation may be prone to errors, especially in noisy data sets. This process is often subject to human choice of threshold, which can be selected incorrectly or may vary across the sample due to brightness changes in the scan data. Therefore continued efforts at different semi-automated segmentation methods are crucial.

Density determination by microCT is possible based on greyscale calibrations, to obtain physical density measurements directly from scan data. However, this method is not routinely used as it involves accurate calibration of the greyscales, for each scan parameter change, and due to potential changes in X-ray intensity and detector sensitivity from the microCT system. Typically, some form of grey-value calibration must be done, using well-defined reference objects (phantoms) in the same scan as the object under investigation. This concept has been demonstrated previously for cements [45,46], but is not widely in use. A similar but slightly improved method has been applied to density calibration for low-density polymer and biological samples using a series of known calibration samples, where differences of 0.1 g/cm^3 could be quantified [47], and using dual energy CT to identify the validity of the calibration, depending on the atomic composition of the materials investigated [48]. The main limitation of the method is the greyscale differences induced by chemical composition differences between the reference materials and the object investigated. To overcome this limitation, it is possible to use the volumetric measurement from microCT data of the material and scale mass, to determine mean density. This method has been demonstrated recently in a methodology paper in [49].

While the absolute density determination of each constituent is not always necessary, it is important to be able to distinguish between aggregate, bitumen and air/voids, for example. The smaller the sample is, and the lower the voltage that can be employed, the better the material discrimination as a general rule. Fig. 3 shows a 70 mm diameter asphalt core sample, with a basic segmentation indicating aggregates in yellow, bitumen in green and pores spaces in blue. This segmentation process can be achieved using a variety of image analysis methods, but the simplest is manual thresholding. For more details of image analysis methods the reader is referred to [7,50–52]. A point to note here is that generally, the best magnification is achieved by scanning one sample at a time. In some cases when resolution and image quality is not crucial, faster scanning is possible, up to a few minutes per sample as demonstrated in [36] for a concrete cylinder. The other option is to scan numerous samples in one scan volume – the disadvantage is reduced X-ray penetration and associated image quality, as well as poorer resolution. However, if samples are small and requirements are not stringent, this can be a very cost effective solution as described in [38].

The imaging of water in microCT scan data has been the topic of extensive investigation in various material types and is not usually possible due to the low attenuation coefficient of water for X-ray

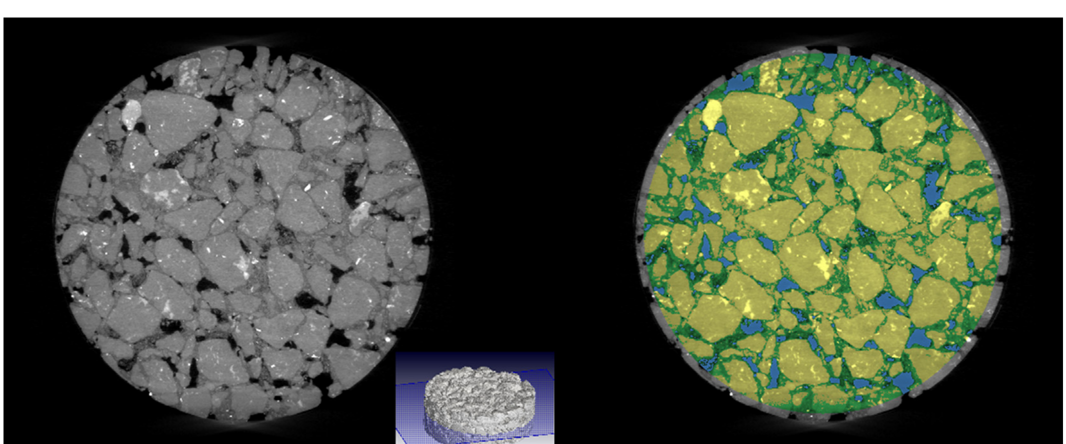

Fig. 3. Segmentation of asphalt sample into pore space (blue), bitumen (green) and aggregate (yellow). (For interpretation of the references to colour in this figure legend, the reader is referred to the web version of this article.)

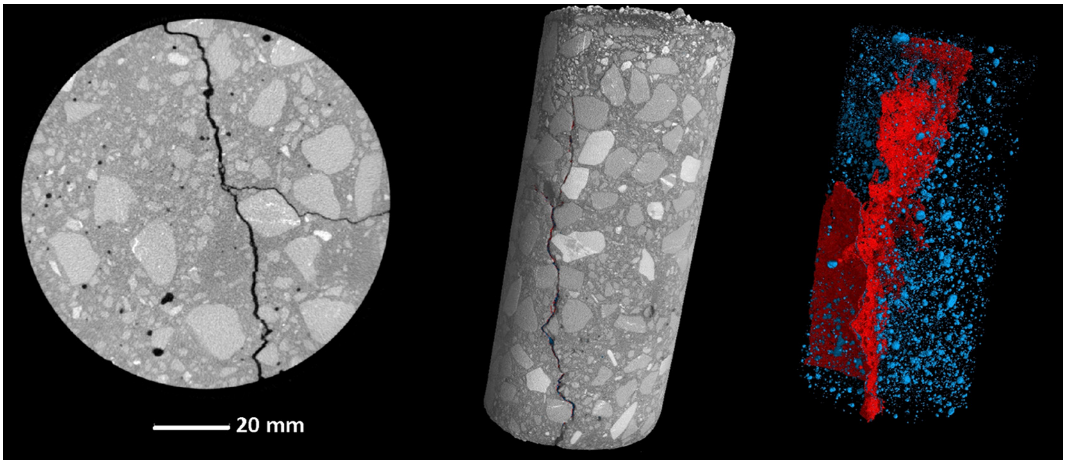

Fig. 4. Cracking in concrete core, shown as (a) central CT slice image, (b) 3D surface view, (c) 3D crack and porosity view, example from [60].

radiation. Nevertheless, the comparison of images of asphalt concrete saturated and dry allowed the analysis of water evaporation in [53]. It was also shown to be possible to distinguish water from similar density host material using a dual energy microCT method [54]. Due to the complexity of concrete-based material compositions this method is not the best way to visualize water content. The use of tracers in the water is more likely to work as demonstrated in [55]. Another option, instead of X-rays, is neutron radiography and neutron tomography which may be used as shown in [56]. Neutrons are very strongly absorbed by water and this makes for high contrast imaging of water distribution. The other advantage is that neutrons have high penetrating power, making it possible to image large samples. The disadvantage is the complexity of such systems (especially the safety requirements) and the general lack of easily accessible neutron facilities. For a recent review of neutron radiography and tomography, the reader is referred to [57].

Phase identification and density determinations using X-ray imaging and microCT are envisaged to continue playing an important fundamental role in understanding the 3D distribution of different components in asphalt and concrete mixes. It is envisaged that the absolute density determination of uniform materials can be useful, for example to characterize aggregates or bitumen separately, for example.

3.3. Damage and failure analysis

Structural damage of concrete and asphalt can occur in many forms, but the most common damage observed is cracking. Damage can also be in the form of surface degradation, for example freeze-thaw damage, internal swelling, e.g. alkali silicate reaction [58,59], or corrosion of steel reinforcing, which subsequently causes cracking and spalling. X-ray CT has been used in the past to determine the cause and extent of damage to concrete, but has mostly been limited to research in laboratories rather than on-site or industrial investigations. A simple CT slice image of a concrete core of 200 mm high by approx. 60 mm diameter, is shown in Fig. 4, this is taken from an industrial project but some images are shown in [60]. As shown in this image, cracking is distinctly different from porosity, and identified as planar connected features.

X-Ray CT was used to determine the level of damage in concrete, with crack tortuosity measured in [61] and similarly in [55], as well as for cracks caused by freeze thaw cycles as measured in [62]. This latter study made use of drilled cores from an existing concrete channel and evaluated the significant freeze thaw damage by using both X-Ray CT and acoustic emission testing. The X-Ray CT data was used to determine the level of damage by calculating average CT numbers. This correlated well with the acoustic emission results of the samples during compressive testing. In another study it was demonstrated that X-Ray CT can be successfully used for determining the damage caused by freeze thaw cycles [63]. They used different mortar samples (conventional, air entrained, with and without fly ash) exposed to freeze thaw cycles. The samples were cylinders 24 mm high and 12 mm in diameter. The air void distribution of the samples were easily captured using the X-Ray CT scan and the quantification of the internal damage, especially the internal cracking and increased void connectivity due to the freeze thaw action was performed.

Determining the extent of internal cracking in concrete can be a useful diagnostic and research tool. Self-healing of cracks in concrete is a relatively new field of research [64–66]. The determination of the effectiveness of self-healing of internal cracks has been a problem as only the surface can be viewed. X-Ray CT has made it possible to determine the internal self-healing capabilities in situ. One example is the work of [67] where bacterial-based self-healing was applied by use of hydrogel spores encapsulated bacterial spores (bio-hydrogels). The internal cracking of control samples (hydrogels) was compared to the performance of samples with bio-hydrogels. It was easy to determine that the bio-hydrogel resulted in a higher level of self-healing. Internal cracks of up to 0.5 mm was bridged by the bio-hydrogel. Another study [68] also looked at the effect of the addition of micro-capsules on the self-healing of cracking causes by reinforcement corrosion while [69] used microCT to determining the self-healing ability of superabsorbent polymers in concrete.

Cracking is common in concrete structures, but the problem is that it can normally only be viewed from the surface and the internal cracking intensity and pattern are unknown. Using X-Ray CT the internal cracking can now be viewed. Transport tracers can be used to determine the internal crack pattern, e.g. [55], and then linking that to diffusion. Cesium carbonate was used as the tracer and it was found that even though the majority of the cracks were captured, the tracer fluid didn't reach all the cracks. Due to the data obtained by X-Ray CT they could link the crack width and crack constrictivity to the diffusion. Similar work has also been done by [70] who used cesium chloride as the tracer in the water. They found this method to be successful in monitoring the flow of water through uncracked mortar.

Sulphate attack can degrade concrete and cause significant damage and is common in concrete sewerage pipes [71]. In a different study the effect of combined sulphate attack and drying wetting cycles on the damage of the concrete samples was investigated [72]. They used X-Ray CT to determine the development of both the internal voids and their connectivity. One of their conclusions was that the damage started in the inside of the specimen, not from the outside. This would have been difficult to detect if X-Ray CT was not used. Similar tests were conducted in [73], but this time comparing the damage of conventional concrete and concrete containing recycled concrete aggregates (RCA). It was found that the RCA improved the resistance to sulfate attack. The improvement was due to the higher water absorption of the RCA which caused a denser structure, however it was also mentioned that the higher porosity and defects of RCA may result in a poorer performance.

Steel rebar corrosion inside cement paste samples was investigated by microCT in [74], where the corrosion products could be identified and quantified, and the corrosion-induced cracking also observed. The bulk of the corrosion was measured at the site of cracking. A similar study investigated the corrosion of steel bar inside concrete samples over a 12 week period, comparing results with electrochemical techniques and measuring volumetric material loss using microCT [75]. The ability to visualize corrosion on steel bars inside concrete allows unique perspectives and identification of corrosion in situ, as demonstrated in [76]. In this study corrosion stains were observed in the concrete around the steel bar, and the corrosion pits could be visualized with exceptional clarity.

Many more studies used microCT for damage detection due to reinforcement corrosion, e.g. [68,77,78]. Carbonation, a known precursor of corrosion, happens from the exposed surface inwards. When the carbonation front reaches the reinforcing, the corrosion is typically initiated. Two different studies used microCT to determine the depth of carbonation in concrete [79,80]. Chloride ion ingress into concrete has the same effect of carbonation as it initiates the steel corrosion once it reaches the reinforcing. In the study by [81] they used microCT effectively to determine the extent of ingress of chlorides in concrete.

As clearly demonstrated in this section, the visualization of failure in concrete materials is one of the major advantages of microCT, as the non-destructive viewing of cracks or degradation allows unique insights into the causes of these issues. One of the future opportunities is in multi-scale CT investigations, ie. subsequent to initial overall scan of a sample, a small internal section can be identified and scanned at higher resolution. This has become more common using improved hardware and software tools in commercial microCT systems (eg. off-axis rotation centre, coupled with region-of-interest scan – ie. field of view is not limited by sample size). Another development is the use of helical scan trajectory and associated reconstructions, which allow improved data quality (less artefacts in images), thereby improving the available field of view of existing hardware (for the same detector size and geometrical magnification). The use of microCT for failure analysis is therefore set to grow as these capabilities are more widely appreciated and the associated newer techniques are implemented more widely.

3.4. Fibre reinforcement

Concretes are often reinforced by a variety of fibres ranging from polymers to steel fibres, of varying lengths, geometries and volumes reinforced. The aim of the fibre is mostly to increase the post cracking tensile strength of the concrete and add general ductility. Fibre reinforcement is still a topic of ongoing research and development [82]. One obvious use of microCT is to visualize the extent and distribution of fibres in the material, as mentioned in the review of industrial microCT applications [3].

In a detailed study in [83], the distribution of steel fibres in concrete samples were investigated. It was shown that with poor design and mixing, fibres can sink to the bottom of the mixture resulting in an unwanted inhomogenous fibre distribution. The fibres near the surfaces in those samples with high fibre content lead to many fibres following the edge profile, also an unwanted effect. This study indicated the ability to quantify the fibre orientations and distributions, which can be very useful to optimize mixing ratios and times. This study was conducted using medical CT with voxel sizes in the region of 1 mm, which is very interesting. Medical CT is not typically used for accurate dimensional measurements and is mainly aimed at imaging only. However, as demonstrated in this study, medical CT provides sufficiently high quality images to analyze fibre orientations and distribution in reasonably large samples. This has also been demonstrated previously in [84] where medical CT and industrial microCT were directly compared on the same samples of concrete, for porosity analysis and reinforcement fibre distribution and orientation analysis.

A detailed microCT study investigated 100 mm diameter samples for porosity and fibre orientation and fibre density, and correlated this information with mechanical test results [85]. It was found that fresh samples contain bubbles towards the top and fibres towards the bottom of the sample, which leads to lower yield strength in mechanical tests.

Similar work was conducted in concrete samples subjected to 3-point bend tests, to better understand the role of the fibres in the failure process, as reported in [86]. Some ongoing work on the same type of samples is shown in Fig. 5 where the mechanical testing is done in static and fatigue modes and the behaviour of the fibres in relation to the concrete cracking can be observed at any stage of testing. This work is still ongoing but Fig. 5 clearly shows the value of the 3D visualization of the fibres (with angular colour coding). It is possible to count the number of fibres crossing the notch area, and it is expected that the number of fibres and the orientation of the fibres strongly affect the mechanical properties.

A great number of other studies successfully determined the steel fibre orientation/dispersion in the concrete, namely [87,88,97–100,89–96]. This was even done for synthetic fibres [98,101] which is more complex due to the similarity of the density of the fibres and the matrix. MicroCT thus has become a very handy tool for visualising the internal distribution of fibre in fibre reinforced concrete.

In a recent study of polymer fibre pullout from concrete test specimens, the use of microCT allowed accurate measurement of the actual pullout distance, indicating significant fibre elongation [102]. A similar study was performed investigating the pullout and crack behaviour of steel fibres using microCT [103].

The internal void distribution of fibre reinforced concrete is also important as often more voids are present when fibres are added. The following studies successfully looked at the internal void structure of fibre reinforced concrete [100,104–107]. The evolution of the cracking of fibre reinforced concrete has also been investigated [108].

It is expected that this capability to visualize and analyze fibres inside the concrete material will add value to future development work for creating optimized composite fibre reinforced concrete materials. As building materials developments moves towards lightweight and ultra high performance concrete materials, fibre reinforcement and the optimization thereof will become increasingly important.

3.5. Temporal evolution or time lapse studies

The non-destructive capability of microCT allows time-lapse or so-called 4D studies, allowing the visualization and analysis of changes occurring in a sample. The advantage of this is that the

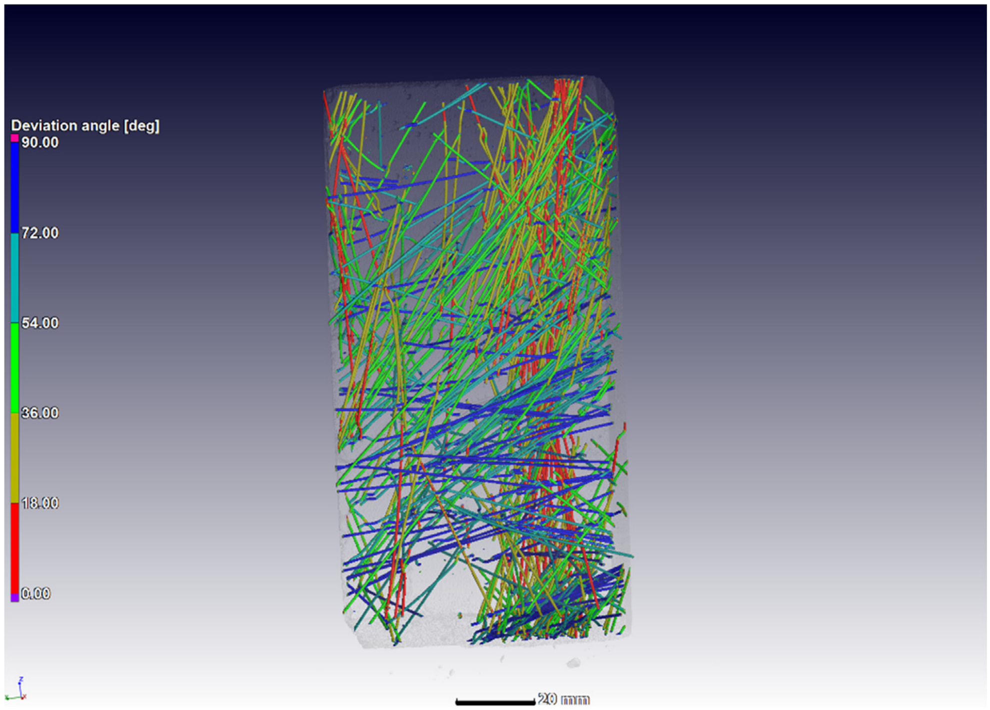

Fig. 5. Steel fibres in concrete beam analyzed for angular orientation (indicated by the colour coding) and 3D distribution.

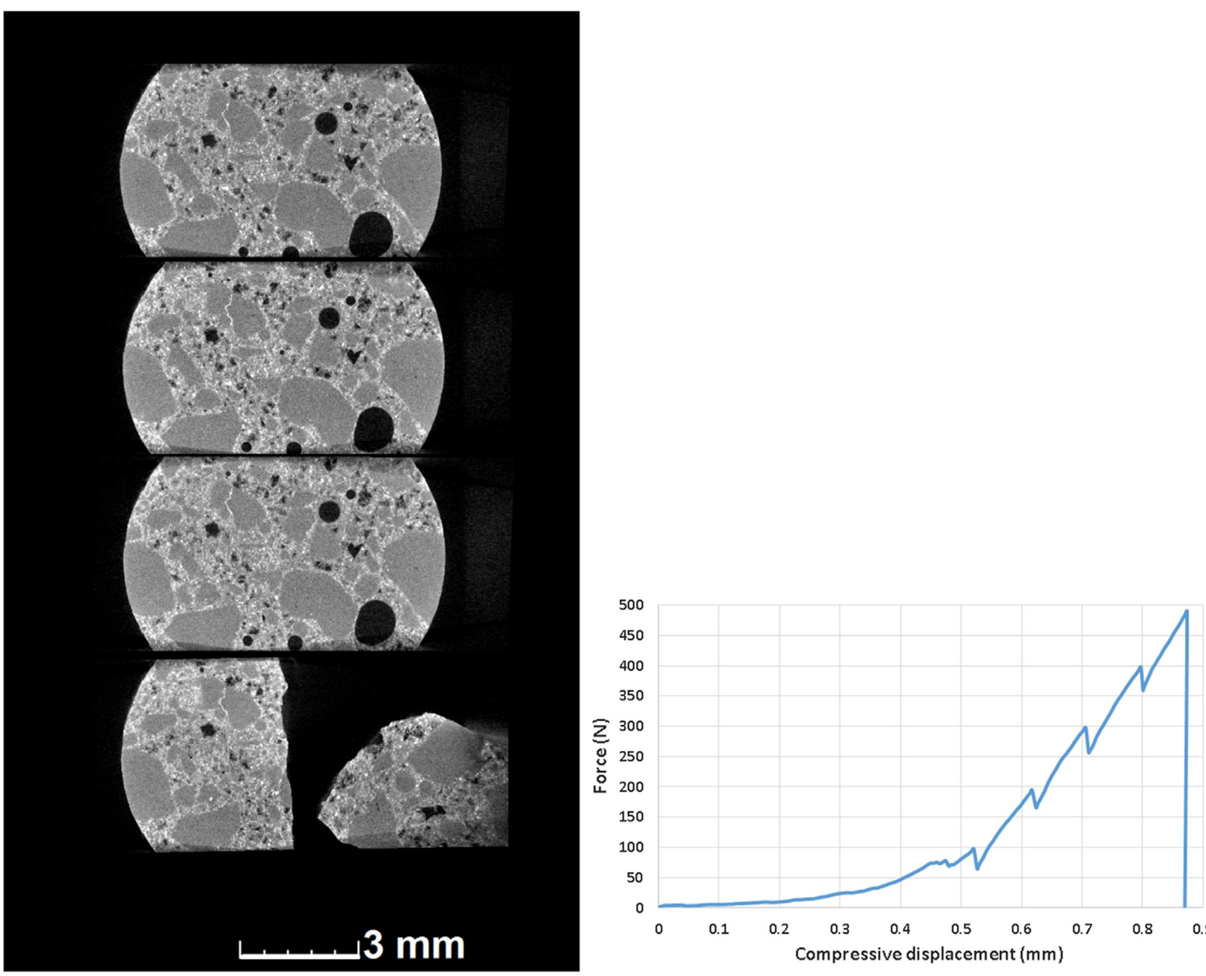

Fig. 6. An 8 mm disk-shaped sample (the same as in Fig. 2) was subjected to in-situ loading and microCT scans at progressively higher loads. Imaged here are the aligned slices at 200 N, 300 N, 400 N and after failure at 490 N. The force-displacement curve shows the steps where the test was stopped for microCT scans.

exact changes can be directly monitored rather than relying on large numbers of samples and sectioning. Already mentioned in section 3.3 is the temporal monitoring of changes induced by freeze–thaw cycles, sulphate attack, self-healing processes and steel bar corrosion. Another obvious application is the visualization of leaching processes. Leaching of cement materials has been investigated by high resolution synchrotron CT, where the formation of microcracks due to the leaching process was observed using time-lapse CT of leached cement samples [109]. This microcracking in the cement material was explained by the reduction in the strength of the cement material around rigid aggregates, and confirmed by simulations.

Corrosion behavior of self-compacting lightweight concrete was investigated in [110]. In particular the chloride-induced reinforcement corrosion was investigated, using microCT to confirm differences in rheological and mechanical performance based on image analysis. Temperature induced damage was investigated by microCT of cement paste samples in [111], where crack initiation was observed at 600 °C and massive fracturing occurred above 900 °C. Water drying from porous asphalt was studied by time-lapse CT in a series of scans over 60 h [53]. In this work the water loss was carefully followed in 3D images, and non-uniform drying behavior could be correlated with water caps in pore spaces near the surface which, when removed, increase the drying rate.

In-situ microCT of concrete cubes under compressive loading was investigated by [112], indicating the ability of the microCT images and associated digital volume correlation to accurately follow fracture evolution. In addition, image-based simulations were used to obtain elastic modulus values which compared very well to that obtained from digital volume correlation. Similar work was also done by [113] and [114]. An example of in-situ compressive loading and microCT imaging of a sample is shown in Fig. 6. In this case a 500 N load cell is used, and full microCT scans recorded at different loading forces (in this case 200, 300, 400 and 500 N). The slice images from scans at each loading condition are vertical cross-sections, aligned to show the same slice position in each scan. The sample in this case failed at 490 N, but no cracks were observed at the scan prior to failure at 400 N. Also observed in this case is that the failure occurs right through one of the larger aggregate stones, an interesting result.

Time-lapse imaging of the same sample is clearly one of the major advantages of the microCT technique, with the simplest being the imaging of a sample at various stages of failure or degradation, scanned at different time steps to monitor the progression of failure. This stepwise scanning can be done by scanning the sample at predefined time steps ex situ, or using in-situ compression, tensile or temperature stages. The major challenge at this point is the large data sets and aligning all these data sets in a practical and simple manner.

3.6. Image based simulations and modelling

Simulations are often used to predict material properties, investigate structure-property relationships and obtain new insights into material behaviour. The advantage of simulation is that the level of complexity can be varied and the property can be analysed independent of other variables, in a cost effective manner compared to physical laboratory tests. However, often the simulations may be too simplistic or may be very computationally intensive or even impossible. Both of these latter issues are being constantly improved as the detail obtained by microCT allows improvement of the models, with real morphological inputs, while computational resources have improved tremendously in the last few years and continue to improve with cloud-based and other supercomputer or distributed computing resources becoming more readily available. Two of the most important simulation types which are relevant to direct simulation using microCT data, are mechanical simulations and absolute permeability simulations, which are described below in more detail. Not discussed here are thermal conductivity and gas diffusion, both of which find little application in concrete and asphalt materials, at least at the micro and macro scales accessible to the microCT technique.

3.6.1. Mechanical simulation

Micromechanical structural mechanics simulations make it possible to highlight stress distributions around and between pores and thereby highlight locations of possible failure and crack formation, as demonstrated for high resolution microCT images [115]. Micromechanical simulations of concrete and asphalt materials, based on CT images, have mostly been done using medical CT scanners at 1 mm resolution, as demonstrated for asphalt in [116,117] for example.

In an early work by Landis and Bolander [118], the fracturing of concrete with and without aggregates were analyzed by in-situ

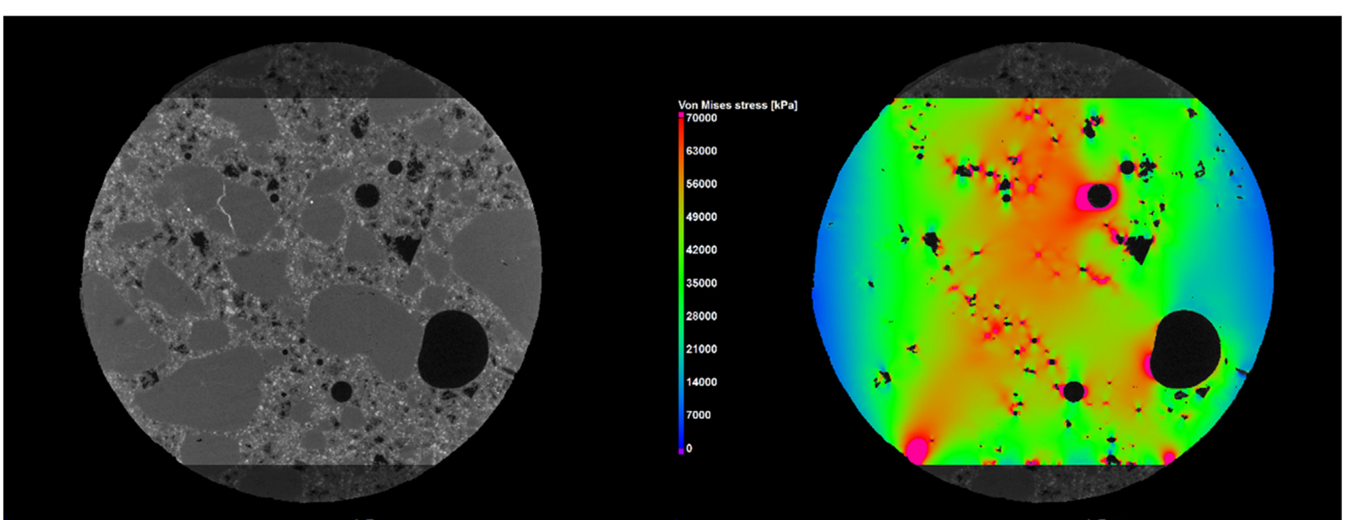

Fig. 7. Structural mechanics simulation – voxel based finite element simulation of elastic compression, based on homogenous elastic properties for cement and aggregate combined. Highest stress area along centre and around pores are shown as expected for this type of sample. This is also the location of fracture when subjected to compression as shown in Fig. 6.

microCT and the presence of the aggregate particles showed in 3D the more complex fracture paths. This was extended to demonstrate how to incorporate information from microCT data of such materials in continuum simulation models. Another example of image-based simulation is given in [35] where binarized microCT images of foamed concrete were used as a basis for simulations of thermal conductivity and compressive elastic modulus and strength. Details of the procedure are not provided but the study clearly indicates the power of this methodology, to investigate material properties based on 3D images.

Cracks can also be determined in concrete samples and then used as input data for mechanical and other analyses. One such example is that of [119] where the internal void structure of a cube splitting test sample was determined using X-Ray CT and used as the geometric input for a 3D finite element analyses. Damage-plasticity was used as a material model and reasonable results were found when comparing the actual and numerical strengths and crack patterns. Analyses in 2 dimensions using inputs from microCT scans has also been performed [120–122] on notched beams tested using a three point bending setup. The concrete was modelled as a four phase material using a continuum damage approach and it was found that the interface transition zone (ITZ) was the dominant influence in the results. The cracks propagated through the ITZ rather than the air voids as one would expect. Similar work has also been done by [123]. Mechanical simulations based on microCT scans of asphalt materials have also been performed with one example being the investigation of chip seal models as reported in [124].

An example is shown in Fig. 7, which is based on the data of the experiment in Fig. 6 described in the previous section – a concrete disk-shaped sample subjected to compression testing and microCT imaging. In this case the unloaded sample data is subjected to micromechanical simulation – an area at the bottom is fixed in all degrees of freedom and load applied in compression to the top area. The simplistic simulation assumes a two-material model of material and air. The stress distributions in this case are mainly along the centre of the specimen and this correlates to the final failure location as expected.

While these studies demonstrate the utility of 3D image-based mechanical simulations, the current capability for microCT resolution coupled with more computing power allow for much more detailed simulations in many cases. These more advanced simulations will in future further advance the understanding of the roles of microporosity, aggregates and binder materials and their interfacial zones on the mechanical properties of concrete and asphalt materials.

3.6.2. Permeability & pore network tortuosity

One of the first microCT-based measures of permeability and tortuosity of a pore network in concrete materials at high resolution was by [125], where they used synchrotron radiation combined with 3D random walk simulations to determine the tortuosity and permeability of the pore network. They found that as the cement paste hardens over 28 days, the porosity and pore connectivity reduces, increasing the tortuosity.

A study by Wang & Dai [126] recently indicated the capability of microCT-based simulation of permeability and diffusivity of cement mortar mixes, eliminating or reducing the need for extensive lab-based testing of such properties. This study was performed using 10 mm cube samples, and small sections used for simulation. It was mentioned that simulation results for permeability are under-estimated due to smallest pore spaces and pore throats being missed in the microCT data, but that this provides useful relative information for materials design purposes. In a study by [55], the diffusivity of concrete samples could be followed using tracers and microCT scans.

This technique is particularly suitable and useful for asphalt characterization. While microCT has resolution limits as mentioned above, which makes small pores and small pore connections invisible to the microCT images, large pore spaces and connected macroporosity, such as that found in typical asphalts can be analyzed for connectivity and permeability. This is done using an image-based laminar flow simulation, illustrated in Fig. 8 for a typical asphalt sample: 70 mm diameter disk-shaped sample. The interest is to understand the permeability and its vertical and horizontal differences, and especially to compare different samples. In

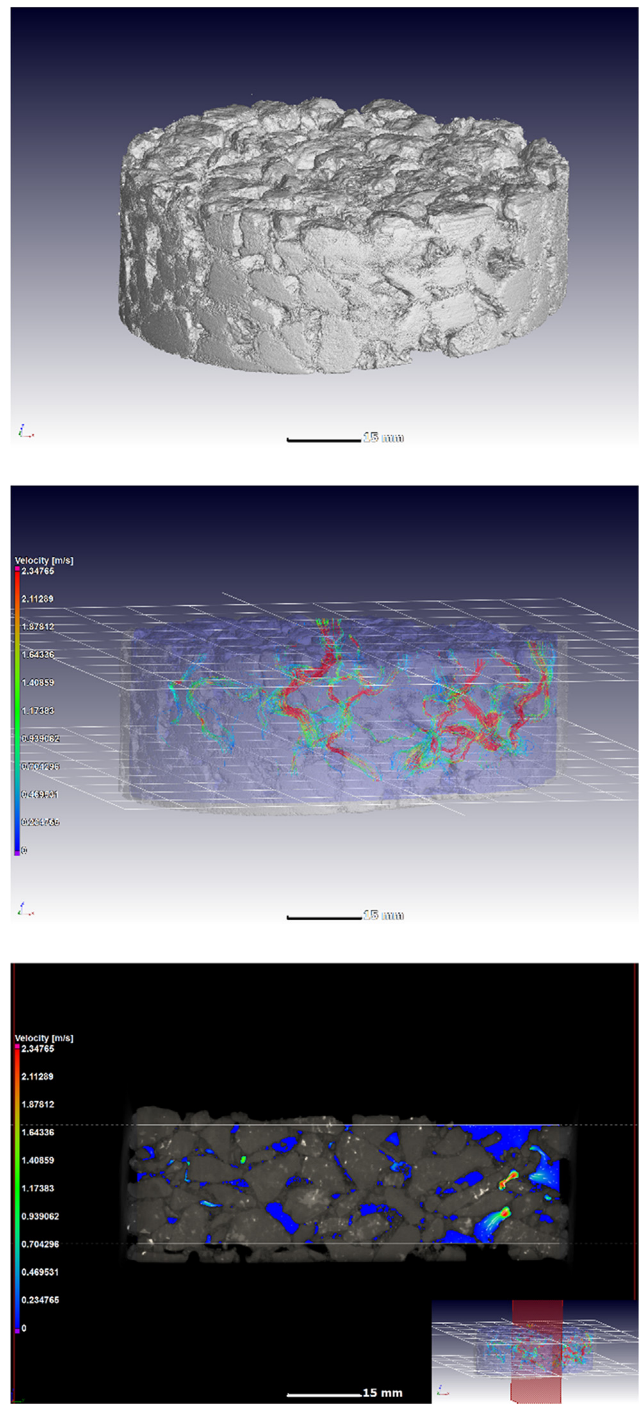

Fig. 8. Asphalt permeability simulation, showing (a) the entire 70 mm-diameter disk-shaped asphalt sample, (b) 3D image of streamlines corresponding to highest-velocity flow and highest mass transport, (c) 2D slice image showing the flow paths in the void spaces between aggregates, bitumen and cement.

this example the simulation is demonstrated vertically, with strongest flow paths visualized in 3D, and velocity profiles shown in the 2D slice image.

The simulation of permeability and pore network connectivity analysis is especially useful for characterization of asphalt materials as mentioned above, and this capability can be used to improve asphalt designs and monitor changes in their permeability behaviour over time, but important attention must be given to obtain similar image quality and apply similar simulation parameters when comparing different samples. Some form of standardization will be required if this is to be used more widely for comparative purposes.

4. Summary and perspectives

As has been demonstrated in this review, the use of microCT for characterization of concrete and asphalt materials has matured to the point where the following summarizes the current state of the art:

- Medical CT scans are sometimes used quite successfully in numerous studies, despite the higher accuracy of microCT scans. Medical CT is still more widely available and allows a larger sample to be scanned in a much reduced time compared to microCT. This makes it particularly useful for quick testing of large numbers of samples, as the scan time is typically a few seconds only. Despite the resolution limits, fibre orientations, large pores and large cracks can be easily visualised.
- MicroCT is already widely used for the 3D analysis of porosity of small concrete samples, which can be termed a "routine" analysis type
- Its use for other applications is relatively underutilized thus far, but is set to grow in usage
- Latest developments in hardware and software associated with microCT have improved the quality and simplicity of obtaining quantitative results from the technique
- Advanced applications which may find particular use in the area of concretes and asphalt are image-based permeability simulations, and structural mechanics simulations or finite element modelling of the microCT data. More advanced porosity analyses (eg. local porosity hotspots or clustering) and their correlation with actual mechanical properties or fracture behavior (eg using time-lapse CT) also holds great promise for improved understanding of material properties.
- Image analysis of a microCT scan is often still the limiting step, requiring complex procedures, custom development or user-defined influence in selecting a material threshold for segmentation. This step is often a bottleneck and may hamper the larger-scale use of the technique, therefore advances in automated analysis and standard methodologies are required
- Besides image analysis, the other limiting factor is the lack of understanding of the technique, which results in incorrect sampling or scan resolution for a particular application. It is not always realized that a microCT scan can be done in many different ways.
- Related to the above, standardization is lacking in the field, especially with regards to sample sizes (and hence resolution limits) for different application types, and the associated methods for image analysis, which can be standardized for each application. In a first attempt towards this standardization goal, some scan strategies are suggested below in Table 1 for different applications.

Table 1
Proposed sampling and scanning strategies.

Information required	Sample type	Scan method	Expected results
Bulk visualization of fibres, large cracks, aggregates and major pore spaces	Large samples up to 2 m long and 500 mm wide	Medical CT, scan time ~10 s	Images of interior of sample, can be used for qualitative viewing only in most cases.
Bulk visualization of fibres, large cracks, aggregates and major pore spaces	Up to 300 mm cores	High voltage and current, strong beam filters, long scan times	Images of interior of sample, can be used for qualitative viewing only in most cases. Quantitative analysis of large features are possible
Macro porosity	30–100 mm core diameter	Fast/medium scan quality	Macroporosity, for statistical comparison – total porosity, max pore size, pore size distribution
Macro permeability	~70 mm core/disk diameter	High quality	Macroporosity, permeability simulation valid for large pore spaces
Micro porosity	1–25 mm core	Very high quality settings required, long scan times	Microporosity, all pores >1.5–75 μm diameter pores quantified, depends on sample size Detailed permeability simulation and pore network visualization possible
Fibre reinforced concrete visualization and analysis	5–50 mm diameter core	High quality	Visualization of fibres in 3D, image processing may allow quantitative analysis of fibre angles, lengths, etc.
Failure analysis investigations	Suggest multiscale investigation: scan large sample, view data, section area of interest, scan at higher resolution and continue this process.	High quality, multiple scans	Multiple scans provide overview and sequential higher resolution images of area of interest. These can be overlapped.
Time lapse studies	Any of above sample sizes	As above	Before-after scans can be overlapped virtually and viewed for comparison in aligned CT slice images, followed by quantitative comparison of 3D measurements

*Fast, medium, high quality and long scan times refer to approximately 20 min, 1 hr, 2 hrs and 4 hrs or more. This includes typical scan times only, sample setup and post-scan reconstruction and analysis is excluded and can vary significantly depending on computing hardware and software available.

Conflict of interest

The authors declare that they have no conflict of interest to this work.

References

[1] E. Maire, P.J. Withers, Quantitative X-ray tomography, Int. Mater. Rev. 59 (2014) 1–43, https://doi.org/10.1179/1743280413Y.0000000023.

[2] V. Cnudde, M.N. Boone, High-resolution X-ray computed tomography in geosciences: a review of the current technology and applications, Earth-Science Rev. 123 (2013) 1–17, https://doi.org/10.1016/j.earscirev.2013.04.003.

[3] L. De Chiffre, S. Carmignato, J.-P. Kruth, R. Schmitt, A. Weckenmann, Industrial applications of computed tomography, CIRP Ann. – Manuf. Technol. 63 (2014) 655–677, https://doi.org/10.1016/j.cirp.2014.05.011.

[4] J.P. Kruth, M. Bartscher, S. Carmignato, R. Schmitt, L. De Chiffre, A. Weckenmann, Computed tomography for dimensional metrology, CIRP Ann. – Manuf. Technol. 60 (2011) 821–842, https://doi.org/10.1016/j.cirp.2011.05.006.

[5] A. du Plessis, I. Yadroitsev, I. Yadroitsava, S. le Roux, X-ray micro computed tomography in additive manufacturing: a review of the current technology and applications, 3D Print. Addit. Manuf. 0 (n.d.).

[6] L. Schoeman, P. Williams, A. du Plessis, M. Manley, X-ray micro-computed tomography (μCT) for non-destructive characterisation of food microstructure, Trends Food Sci. Technol. 47 (2016) 10–24, https://doi.org/10.1016/j.tifs.2015.10.016.

[7] A. du Plessis, C. Broeckhoven, A. Guelpa, S.G. le Roux, Laboratory x-ray micro-computed tomography: a user guideline for biological samples, GigaScience 6 (2017) 42–49, https://doi.org/10.1093/gigascience/gix027.

[8] M.A. Vicente, J. Mínguez, D.C. González, The use of computed tomography to explore the microstructure of materials in civil engineering: from rocks to concrete, Comput. Tomogr. – Adv. Appl., InTech (2017), https://doi.org/10.5772/intechopen.69245.

[9] E. Masad, X-ray computed tomography of aggregates and asphalt mixes 62 (2004) 775–783 (accessed March 14, 2018) https://www-scopus-com.ez.sun.ac.za/record/display.uri?origin=recordpage&eid=2-s2.0-3843076332&citeCnt=200&noHighlight=false&sort=plf-f&src=s&st1=Characterization+of+Air+Void+Distribution+in+Asphalt+Mixes+using+X-ray+Computed+Tomography&st2=&sid=a83714603bd0937629fc4728c81c7dc3&sot=b&sdt=b&sl=105&s=TITLE-ABS-KEY%28Characterization+of+Air+Void+Distribution+in+Asphalt+Mixes+using+X-ray+Computed+Tomography%29&relpos=4.

[10] E. Masad, V.K. Jandhyala, N. Dasgupta, N. Somadevan, N. Shashidhar, Characterization of air void distribution in asphalt mixes using X-ray computed tomography, J. Mater. Civ. Eng. 14 (2002) 122–129, https://doi.org/10.1061/(ASCE)0899-1561(2002) 14:2(122).

[11] E. Masad, B. Muhunthan, N. Shashidhar, T. Harman, Internal structure characterization of asphalt concrete using image analysis, J. Comput. Civ. Eng. 13 (1999) 88–95, https://doi.org/10.1061/(ASCE)0887-3801(1999) 13:2(88).

[12] V. Boel, V. Cnudde, G. De Schutter, P. Jacobs, Exploring the potential of x-ray tomography in microstructural studies of cementitious systems, 2nd Int. Symp. Adv. Concr. through Sci. Eng. (2006) (accessed May 7, 2018) https://pdfs.semanticscholar.org/c19b/2c00a85015908695c204a0b255a8363192c2.pdf.

[13] S.R. Stock, X-ray microtomography of materials, Int. Mater. Rev. 44 (1999) 141–164, https://doi.org/10.1179/095066099101528261.

[14] S. Lu, E.N. Landis, D.T. Keane, X-ray microtomographic studies of pore structure and permeability in Portland cement concrete, Mater. Struct. 39 (2007) 611–620, https://doi.org/10.1617/s11527-006-9099-7.

[15] A. du Plessis, S.G. le Roux, A. Guelpa, Comparison of medical and industrial X-ray computed tomography for non-destructive testing, Case Stud. Nondestruct. Test. Eval. (2016), https://doi.org/10.1016/j.csndt.2016.07.001.

[16] S.R. Stock, Recent advances in X-ray microtomography applied to materials, Int. Mater. Rev. 53 (2008) 129–181, https://doi.org/10.1179/174328008X277803.

[17] V. Cnudde, A. Cwirzen, B. Masschaele, P.J.S. Jacobs, Porosity and microstructure characterization of building stones and concretes, Eng. Geol. 103 (2009) 76–83, https://doi.org/10.1016/J.ENGGEO.2008.06.014.

[18] G.N. Hounsfield, Computerized transverse axial scanning (tomography): Part 1. Description of system, Br. J. Radiol. 46 (1973) 1016–1022, https://doi.org/10.1259/0007-1285-46-552-1016.

[19] A.C. Kak, M. Slaney, Principles of Computerized Tomographic Imaging (Society for Industrial and Applied Mathematics), Soc. Ind. Appl. Math. (2001) (accessed January 19, 2016) http://epubs.siam.org/doi/book/10.1137/1.9780898719277.

[20] L.A. Feldkamp, L.C. Davis, J.W. Kress, Practical cone-beam algorithm, J. Opt. Soc. Am. A. 1 (1984) 612, https://doi.org/10.1364/JOSAA.1.000612.

[21] A. du Plessis, S.G. le Roux, A. Guelpa, The CT Scanner Facility at Stellenbosch University: an open access X-ray computed tomography laboratory, Nucl. Instruments Methods Phys. Res. Sect. B Beam Interact. with Mater. Atoms. 384 (2016) 42–49, https://doi.org/10.1016/j.nimb.2016.08.005.

[22] R. Kumar, B. Bhattacharjee, Porosity, pore size distribution and in situ strength of concrete, Cem. Concr. Res. 33 (2003) 155–164, https://doi.org/10.1016/S0008-8846(02)00942-0.

[23] E.J. Garboczi, D.P. Bentz, Modelling of the microstructure and transport properties of concrete, Constr. Build. Mater. 10 (1996) 293–300, https://doi.org/10.1016/0950-0618(94)00019-0.

[24] S. Diamond, Aspects of concrete porosity revisited, Cem. Concr. Res. 29 (1999) 1181–1188, https://doi.org/10.1016/S0008-8846(99)00122-2.

[25] P. Stroeven, J. Hu, Review paper – stereology: historical perspective and applicability to concrete technology, Mater. Struct. 39 (2007) 127–135, https://doi.org/10.1617/s11527-005-9031-6.

[26] K.Y. Kim, T.S. Yun, J. Choo, D.H. Kang, H.S. Shin, Determination of air-void parameters of hardened cement-based materials using X-ray computed tomography, Constr. Build. Mater. 37 (2012) 93–101, https://doi.org/10.1016/J.CONBUILDMAT.2012.07.012.

[27] T.S. Yun, K.Y. Kim, J. Choo, D.H. Kang, Quantifying the distribution of paste-void spacing of hardened cement paste using X-ray computed tomography, Mater. Charact. 73 (2012) 137–143, https://doi.org/10.1016/J.MATCHAR.2012.08.008.

[28] H. Lu, K. Peterson, O. Chernoloz, Measurement of entrained air-void parameters in Portland cement concrete using micro X-ray computed tomography, Int. J. Pavement Eng. 19 (2018) 109–121, https://doi.org/10.1080/10298436.2016.1172705.

[29] E.E. Bernardes, E.V. Mantilla Carrasco, W.L. Vasconcelos, A.G. de Magalhães, X-ray microtomography (μ-CT) to analyze the pore structure of a Portland cement composite based on the selection of different regions of interest, Constr. Build. Mater. 95 (2015) 703–709, https://doi.org/10.1016/J.CONBUILDMAT.2015.07.128.

[30] H. Lu, E. Alymov, S. Shah, K. Peterson, Measurement of air void system in lightweight concrete by X-ray computed tomography, Constr. Build. Mater. 152 (2017) 467–483, https://doi.org/10.1016/J.CONBUILDMAT.2017.06.180.

[31] N. Bossa, P. Chaurand, J. Vicente, D. Borschneck, C. Levard, O. Aguerre-Chariol, J. Rose, Micro- and nano-X-ray computed-tomography: a step forward in the characterization of the pore network of a leached cement paste, Cem. Concr. Res. 67 (2015) 138–147, https://doi.org/10.1016/j.cemconres.2014.08.007.

[32] Ł. Sadowski, D. Stefaniuk, Microstructural evolution within the interphase between hardening overlay and existing concrete substrates, Appl. Sci. 7 (2017) 123, https://doi.org/10.3390/app7020123.

[33] Ł. Sadowski, D. Stefaniuk, J. Hoła, The effect of the porosity within the interfacial zone between layers on pull-off adhesion, Constr. Build. Mater. 152 (2017) 887–897, https://doi.org/10.1016/J.CONBUILDMAT.2017.07.080.

[34] X. Pang, J. Singh, W. Cuello Jimenez, Characterizing gas bubble size distribution of laboratory foamed cement using X-ray micro-CT, Constr. Build. Mater. 167 (2018) 243–252, https://doi.org/10.1016/J.CONBUILDMAT.2018.02.030.

[35] S.-Y. Chung, C. Lehmann, M. Abd Elrahman, D. Stephan, Pore characteristics and their effects on the material properties of foamed concrete evaluated using micro-CT images and numerical approaches, Appl. Sci. 7 (2017) 550, https://doi.org/10.3390/app7060550.

[36] A. du Plessis, B.J. Olawuyi, W.P. Boshoff, S.G. le Roux, Simple and fast porosity analysis of concrete using X-ray computed tomography, Mater. Struct. 49 (2014) 553–562, https://doi.org/10.1617/s11527-014-0519-9.

[37] S.G. Le Roux, A. Du Plessis, A. Rozendaal, The quantitative analysis of tungsten ore using X-ray microCT: case study, Comput. Geosci. (2015), https://doi.org/10.1016/j.cageo.2015.09.009.

[38] A. Guelpa, A. du Plessis, M. Manley, A high-throughput X-ray micro-computed tomography (μCT) approach for measuring single kernel maize (Zea mays L.) volumes and densities, J. Cereal Sci. 69 (2016), https://doi.org/10.1016/j.jcs.2016.04.009.

[39] B.J. Olawuyi, W.P. Boshoff, Influence of SAP content and curing age on air void distribution of high performance concrete using 3D volume analysis, Constr. Build. Mater. 135 (2017) 580–589, https://doi.org/10.1016/J.CONBUILDMAT.2016.12.128.

[40] S. Laustsen, M.T. Hasholt, O.M. Jensen, Void structure of concrete with superabsorbent polymers and its relation to frost resistance of concrete, Mater. Struct. 48 (2015) 357–368, https://doi.org/10.1617/s11527-013-0188-0.

[41] S. Kang, S. Hong, J. Moon, The effect of superabsorbent polymer on various scale of pore structure in ultra-high performance concrete, Constr. Build. Mater. 172 (2018) 29–40, https://doi.org/10.1016/j.conbuildmat.2018.03.193.

[42] J. Schock, S. Liebl, K. Achterhold, F. Pfeiffer, Obtaining the spacing factor of microporous concrete using high-resolution Dual Energy X-ray Micro CT, Cem. Concr. Res. 89 (2016) 200–205, https://doi.org/10.1016/j.cemconres.2016.08.008.

[43] W.-J. Long, B.-X. Xiao, Y.-C. Gu, F. Xing, Micro- and macro-scale characterization of nano-SiO2 reinforced alkali activated slag composites, Mater. Charact. 136 (2018) 111–121, https://doi.org/10.1016/J.MATCHAR.2017.12.013.

[44] T. Sugiyama, M.A.B. Promentilla, T. Hitomi, N. Takeda, Application of synchrotron microtomography for pore structure characterization of deteriorated cementitious materials due to leaching, Cem. Concr. Res. 40 (2010) 1265–1270, https://doi.org/10.1016/J.CEMCONRES.2009.10.009.

[45] H.Y. Aruntaş, İ. Tekin, R. Birgül, Determining Hounsfield Unit values of mortar constituents by computerized tomography, Measurement 43 (2010) 410–414, https://doi.org/10.1016/J.MEASUREMENT.2009.12.010.

[46] K. Wan, L. Chen, Q. Xu, Calibration of grayscale values of cement constituents using industrial X-ray tomography, Sci. China Technol. Sci. 58 (2015) 485–492, https://doi.org/10.1007/s11431-014-5751-6.

[47] A. Guelpa, A. du Plessis, M. Kidd, M. Manley, Non-destructive Estimation of Maize (Zea mays L.) Kernel Hardness by Means of an X-ray Micro-computed Tomography (μCT) Density Calibration, Food Bioprocess Technol. 8 (2015) 1419–1429, https://doi.org/10.1007/s11947-015-1502-3.

[48] A. Du Plessis, M. Meincken, T. Seifert, Quantitative determination of density and mass of polymeric materials using microfocus computed tomography, J. Nondestruct. Eval. 32 (2013) 413–417, https://doi.org/10.1007/s10921-013-0195-7.

[49] A. du Plessis, Standard method for microCT-based additive manufacturing quality control 2: density measurement, Protocols. Io. (2018). https://www.protocols.io/view/standard-method-for-microct-based-additive-manufac-sbvean6.

[50] T. Matthews, A. du Plessis, Using X-ray computed tomography analysis tools to compare the skeletal element morphology of fossil and modern frog (Anura) species, Palaeontol. Electron. 19 (2016).

[51] Y. Liu, A.M. Kiss, D.H. Larsson, F. Yang, P. Pianetta, To get the most out of high resolution X-ray tomography: a review of the post-reconstruction analysis, Spectrochim. Acta Part B At. Spectrosc. 117 (2016) 29–41, https://doi.org/10.1016/j.sab.2016.01.002.

[52] A. Lavrov, E. Anabela, C. Panduro, M. Torsæter, Synchrotron study of cement hydration: towards computed tomography analysis of interfacial transition zone, Energy Procedia. 114 (2017) 5109–5117, https://doi.org/10.1016/j.egypro.2017.03.1666.

[53] I. Jerjen, L.D. Poulikakos, M. Plamondon, P. Schuetz, T. Luethi, A. Flisch, Drying of porous asphalt concrete investigated by X-ray computed tomography, Phys. Procedia. 69 (2015) 451–456, https://doi.org/10.1016/J.PHPRO.2015.07.063.

[54] O. Lindgren, T. Seifert, A. Du Plessis, Moisture content measurements in wood using dual-energy CT scanning – a feasibility study, Wood Mater. Sci. Eng. 11 (2016), https://doi.org/10.1080/17480272.2016.1201863.

[55] I.S. Darma, T. Sugiyama, M.A.B. Promentilla, Application of X-ray CT to study diffusivity in cracked concrete through the observation of tracer transport, J. Adv. Concr. Technol. 11 (2013) 266–281, https://doi.org/10.3151/jact.11.266.

[56] P. Zhang, F.H. Wittmann, P. Lura, H.S. Müller, S. Han, T. Zhao, Application of neutron imaging to investigate fundamental aspects of durability of cement-based materials: a review, Cem. Concr. Res. 108 (2018) 152–166, https://doi.org/10.1016/J.CEMCONRES.2018.03.003.

[57] N. Kardjilov, I. Manke, R. Woracek, A. Hilger, J. Banhart, Advances in neutron imaging, Mater. Today. (2018), https://doi.org/10.1016/j.mattod.2018.03.001.

[58] S. Guo, Q. Dai, X. Sun, X. Xiao, X-ray CT characterization and fracture simulation of ASR damage of glass particles in alkaline solution and mortar, Theor. Appl. Fract. Mech. 92 (2017) 76–88, https://doi.org/10.1016/j.tafmec.2017.05.014.

[59] S. Guo, Q. Dai, X. Sun, X. Xiao, R. Si, J. Wang, Reduced alkali-silica reaction damage in recycled glass mortar samples with supplementary cementitious materials, J. Clean. Prod. 172 (2018) 3621–3633, https://doi.org/10.1016/j.jclepro.2017.11.119.

[60] A. du Plessis, http://blogs.sun.ac.za/ctscanner/concrete-cracking/, (2014). http://blogs.sun.ac.za/ctscanner/concrete-cracking/ (accessed May 1, 2018).

[61] E. Schlangen, Crack Development in Concrete, Part 1: fracture Experiments and CT-Scan Observations, Key Eng. Mater. 385–387 (2008) 69–72, https://doi.org/10.4028/www.scientific.net/KEM.385-387.69.

[62] T. Suzuki, H. Ogata, R. Takada, M. Aoki, Use of acoustic emission and X-ray computed tomography for damage evaluation of freeze-thawed concrete, Constr. Build. Mater. 24 (2010) 2347–2352, https://doi.org/10.1016/J.CONBUILDMAT.2010.05.005.

[63] M.A.B. Promentilla, T. Sugiyama, X-ray microtomography of mortars exposed to freezing-thawing action, J. Adv. Concr. Technol. 8 (2010) 97–111, https://doi.org/10.3151/jact.8.97.

[64] K. Vijay, M. Murmu, S.V. Deo, Bacteria based self healing concrete–a review, Constr. Build. Mater. 152 (2017) 1008–1014, https://doi.org/10.1016/J.CONBUILDMAT.2017.07.040.

[65] E. Tziviloglou, V. Wiktor, H.M. Jonkers, E. Schlangen, Bacteria-based self-healing concrete to increase liquid tightness of cracks, Constr. Build. Mater. 122 (2016) 118–125, https://doi.org/10.1016/J.CONBUILDMAT.2016.06.080.

[66] B. Hilloulin, K. Van Tittelboom, E. Gruyaert, N. De Belie, A. Loukili, Design of polymeric capsules for self-healing concrete, Cem. Concr. Compos. 55 (2015) 298–307, https://doi.org/10.1016/J.CEMCONCOMP.2014.09.022.

[67] J. Wang, J. Dewanckele, V. Cnudde, S. Van Vlierberghe, W. Verstraete, N. De Belie, X-ray computed tomography proof of bacterial-based self-healing in concrete, Cem. Concr. Compos. 53 (2014) 289–304, https://doi.org/10.1016/J.CEMCONCOMP.2014.07.014.

[68] B. Dong, W. Ding, S. Qin, N. Han, G. Fang, Y. Liu, F. Xing, Chemical self-healing system with novel microcapsules for corrosion inhibition of rebar in concrete, Cem. Concr. Compos. 85 (2018) 83–91, https://doi.org/10.1016/j.cemconcomp.2017.09.012.

[69] D. Snoeck, J. Dewanckele, V. Cnudde, N. De Belie, X-ray computed microtomography to study autogenous healing of cementitious materials promoted by superabsorbent polymers, Cem. Concr. Compos. 65 (2016) 83–93, https://doi.org/10.1016/j.cemconcomp.2015.10.016.

[70] L. Yang, Y. Zhang, Z. Liu, P. Zhao, C. Liu, In-situ tracking of water transport in cement paste using X-ray computed tomography combined with CsCl enhancing, Mater. Lett. 160 (2015) 381–383, https://doi.org/10.1016/J.MATLET.2015.08.011.

[71] M. O'Connell, C. McNally, M.G. Richardson, Biochemical attack on concrete in wastewater applications: a state of the art review, Cem. Concr. Compos. 32 (2010) 479–485, https://doi.org/10.1016/J.CEMCONCOMP.2010.05.001.

[72] J. Yuan, Y. Liu, Z. Tan, B. Zhang, Investigating the failure process of concrete under the coupled actions between sulfate attack and drying–wetting cycles by using X-ray CT, Constr. Build. Mater. 108 (2016) 129–138, https://doi.org/10.1016/J.CONBUILDMAT.2016.01.040.

[73] B. Qi, J. Gao, F. Chen, D. Shen, Evaluation of the damage process of recycled aggregate concrete under sulfate attack and wetting-drying cycles, Constr. Build. Mater. 138 (2017) 254–262, https://doi.org/10.1016/J.CONBUILDMAT.2017.02.022.

[74] B. Dong, G. Fang, Y. Liu, P. Dong, J. Zhang, F. Xing, S. Hong, Monitoring reinforcement corrosion and corrosion-induced cracking by X-ray microcomputed tomography method, Cem. Concr. Res. 100 (2017) 311–321, https://doi.org/10.1016/J.CEMCONRES.2017.07.009.

[75] A. Česen, T. Kosec, A. Legat, Characterization of steel corrosion in mortar by various electrochemical and physical techniques, Corros. Sci. 75 (2013) 47–57, https://doi.org/10.1016/J.CORSCI.2013.05.015.

[76] S. Chandra Paul, G.P.A.G. van Zijl, Crack formation and chloride induced corrosion in reinforced strain hardening cement-based composite (R/SHCC), J. Adv. Concr. Technol. 12 (2014) 340–351, https://doi.org/10.3151/jact.12.340.

[77] J. Shi, J. Ming, Y. Zhang, J. Jiang, Corrosion products and corrosion-induced cracks of low-alloy steel and low-carbon steel in concrete, Cem. Concr. Compos. 88 (2018) 121–129, https://doi.org/10.1016/j.cemconcomp.2018.02.002.

[78] J. Shi, J. Ming, Influence of defects at the steel-mortar interface on the corrosion behavior of steel, Constr. Build. Mater. 136 (2017) 118–125, https://doi.org/10.1016/j.conbuildmat.2017.01.007.

[79] H. Jiande, L. Weiqing, W. Shuguang, D. Dongsheng, X. Feng, L. Weiwei, G. De Schutter, Effects of crack and ITZ and aggregate on carbonation penetration based on 3D micro X-ray CT microstructure evolution, Constr. Build. Mater. 128 (2016) 256–271, https://doi.org/10.1016/j.conbuildmat.2016.10.062.

[80] J. Liu, M. Ba, Y. Du, Z. He, J. Chen, Effects of chloride ions on carbonation rate of hardened cement paste by X-ray CT techniques, Constr. Build. Mater. 122 (2016) 619–627, https://doi.org/10.1016/j.conbuildmat.2016.06.101.

[81] B. Qi, J. Gao, F. Chen, D. Shen, Chloride penetration into recycled aggregate concrete subjected to wetting – drying cycles and flexural loading, Constr. Build. Mater. 174 (2018) 130–137, https://doi.org/10.1016/j.conbuildmat.2018.04.122.

[82] V. Afroughsabet, L. Biolzi, T. Ozbakkaloglu, High-performance fiber-reinforced concrete: a review, J. Mater. Sci. 51 (2016) 6517–6551, https://doi.org/10.1007/s10853-016-9917-4.

[83] G.L. Balázs, O. Czoboly, É. Lublóy, K. Kapitány, Á. Barsi, Observation of steel fibres in concrete with Computed Tomography, Constr. Build. Mater. 140 (2017) 534–541, https://doi.org/10.1016/J.CONBUILDMAT.2017.02.114.

[84] A. du Plessis, S.G. le Roux, A. Guelpa, Comparison of medical and industrial X-ray computed tomography for non-destructive testing, Case Stud. Nondestruct. Test. Eval. 6 (2016), https://doi.org/10.1016/j.csndt.2016.07.001.

[85] R. Wang, X. Gao, J. Zhang, G. Han, Spatial distribution of steel fibers and air bubbles in UHPC cylinder determined by X-ray CT method, Constr. Build. Mater. 160 (2018) 39–47, https://doi.org/10.1016/J.CONBUILDMAT.2017.11.030.

[86] S. Zeranka, Steel fibre-reinforced concrete: multi-scale characterisation towards numerical modelling, (2017). http://scholar.sun.ac.za/handle/10019.1/102734 (accessed May 7, 2018).

[87] B. Zhou, Y. Uchida, Relationship between fiber orientation/distribution and post-cracking behaviour in ultra-high-performance fiber-reinforced concrete (UHPFRC), Cem. Concr. Compos. 83 (2017) 66–75, https://doi.org/10.1016/j.cemconcomp.2017.07.007.

[88] P. Stahli, R. Custer, J.G.M. Van Mier, On flow properties, fibre distribution, fibre orientation and flexural behaviour of FRC, Mater. Struct. (2008) 189–196, https://doi.org/10.1617/s11527-007-9229-x.

[89] E.V. Sarmiento, M.A.N. Hendriks, M.R. Geiker, T. Kanstad, Modelling the influence of the fibre structure on the structural behaviour of flowable fibre-reinforced concrete, Eng. Struct. 124 (2016) 186–195, https://doi.org/10.1016/j.engstruct.2016.05.053.

[90] S. Oldrich, Z. Giedrius, J.E. Bolander, H. Stang, Influence of formwork surface on the orientation of steel fibres within self-compacting concrete and on the mechanical properties of cast structural elements, Cem. Concr. Compos. 50 (2014) 60–72, https://doi.org/10.1016/j.cemconcomp.2013.12.002.

[91] J.-P. Suuronen, A. Kallonen, M. Eik, J. Puttonen, R. Serimaa, H. Herrmann, Analysis of short fibres orientation in steel fibre-reinforced concrete (SFRC) by X-ray tomography, J. Mater. Sci. (2013) 1358–1367, https://doi.org/10.1007/s10853-012-6882-4.

[92] T. Ponikiewski, J. Katzer, M. Bugdol, M. Rudzki, X-ray computed tomography harnessed to determine 3D spacing of steel fibres in self compacting concrete (SCC) slabs, Constr. Build. Mater. 74 (2015) 102–108, https://doi.org/10.1016/j.conbuildmat.2014.10.024.

[93] A.B. Groeneveld, T.M. Ahlborn, C.K. Crane, C.A. Burchfield, E.N. Landis, Dynamic strength and ductility of ultra-high performance concrete with flow-induced fiber alignment, Int. J. Impact Eng. 111 (2017) 37–45, https://doi.org/10.1016/j.ijimpeng.2017.08.009.

[94] T. Ponikiewski, J. Golaszewski, M. Rudzki, M. Bugdol, Determination of steel fibres distribution in self-compacting concrete beams using X-ray computed tomography, Arch. Civ. Mech. Eng. 15 (2015), https://doi.org/10.1016/j.acme.2014.08.008.

[95] B. Zhou, Y. Uchida, Influence of flowability, casting time and formwork geometry on fiber orientation and mechanical properties of UHPFRC, Cem. Concr. Res. 95 (2017) 164–177, https://doi.org/10.1016/j.cemconres.2017.02.017.

[96] A. Orbe, J. Cuadrado, R. Losada, E. Rojí, Framework for the design and analysis of steel fiber reinforced self-compacting concrete structures, Constr. Build. Mater. 35 (2012) 676–686, https://doi.org/10.1016/j.conbuildmat.2012.04.135.
[97] J. Liu, C. Li, J. Liu, G. Cui, Z. Yang, Study on 3D spatial distribution of steel fibers in fiber reinforced cementitious composites through micro-CT technique, Constr. Build. Mater. 48 (2013) 656–661, https://doi.org/10.1016/j.conbuildmat.2013.07.052.
[98] J. Kaufmann, K. Frech, P. Schuetz, B. Münch, Rebound and orientation of fibers in wet sprayed concrete applications, Constr. Build. Mater. 49 (2013) 15–22, https://doi.org/10.1016/j.conbuildmat.2013.07.051.
[99] E.V. Sarmiento, M.R. Geiker, T. Kanstad, Influence of fibre configuration on the mechanical behaviour of standard test specimens and full-scale beams made of flowable FRC, Constr. Build. Mater. 111 (2016) 794–804, https://doi.org/10.1016/j.conbuildmat.2016.02.129.
[100] Y. Xu, J. Liu, J. Liu, P. Zhang, Q. Zhang, L. Jiang, Experimental studies and modeling of creep of UHPC, Constr. Build. Mater. 175 (2018) 643–652, https://doi.org/10.1016/j.conbuildmat.2018.04.157.
[101] P. Pujadas, A. Blanco, S. Cavalaro, A. De Fuente, A. Aguado, Fibre distribution in macro-plastic fibre reinforced concrete slab-panels, Constr. Build. Mater. 64 (2014) 496–503, https://doi.org/10.1016/j.conbuildmat.2014.04.067.
[102] A.J. Babafemi, A. du Plessis, W.P. Boshoff, Pull-out creep mechanism of synthetic macro fibres under a sustained load, Constr. Build. Mater. 174 (2018) 466–473, https://doi.org/10.1016/J.CONBUILDMAT.2018.04.148.
[103] P.D. Nieuwoudt, A.J. Babafemi, W.P. Boshoff, The response of cracked steel fibre reinforced concrete under various sustained stress levels on both the macro and single fibre level, Constr. Build. Mater. 156 (2017) 828–843, https://doi.org/10.1016/J.CONBUILDMAT.2017.09.022.
[104] C. Lu, V.C. Li, C.K.Y. Leung, Flaw characterization and correlation with cracking strength in Engineered Cementitious Composites (ECC), Cem. Concr. Res. 107 (2018) 64–74, https://doi.org/10.1016/j.cemconres.2018.02.024.
[105] A. Qsymah, R. Sharma, Z. Yang, L. Margetts, P. Mummery, Micro X-ray computed tomography image-based two-scale homogenisation of ultra high performance fibre reinforced concrete, Constr. Build. Mater. 130 (2017) 230–240, https://doi.org/10.1016/j.conbuildmat.2016.09.020.
[106] T. Ponikiewski, J. Katzer, M. Bugdol, M. Rudzki, Determination of 3D porosity in steel fibre reinforced SCC beams using X-ray computed tomography, Constr. Build. Mater. 68 (2014) 333–340, https://doi.org/10.1016/j.conbuildmat.2014.06.064.
[107] S. Erdem, A.R. Dawson, N.H. Thom, Microstructure-linked strength properties and impact response of conventional and recycled concrete reinforced with steel and synthetic macro fibres, Constr. Build. Mater. 25 (2011) 4025–4036, https://doi.org/10.1016/j.conbuildmat.2011.04.037.
[108] X.W. Yi, G.W. Ma, A. Fourie, Compressive behaviour of fi bre-reinforced cemented paste back fi ll, Geotext. Geomembranes. 43 (2015) 207–215, https://doi.org/10.1016/j.geotexmem.2015.03.003.
[109] T. Rougelot, N. Burlion, D. Bernard, F. Skoczylas, About microcracking due to leaching in cementitious composites: X-ray microtomography description and numerical approach, Cem. Concr. Res. 40 (2010) 271–283, https://doi.org/10.1016/J.CEMCONRES.2009.09.021.
[110] S. Erdem, X-ray computed tomography and fractal analysis for the evaluation of segregation resistance, strength response and accelerated corrosion behaviour of self-compacting lightweight concrete, Constr. Build. Mater. 61 (2014) 10–17, https://doi.org/10.1016/J.CONBUILDMAT.2014.02.070.
[111] K.Y. Kim, T.S. Yun, K.P. Park, Evaluation of pore structures and cracking in cement paste exposed to elevated temperatures by X-ray computed tomography, Cem. Concr. Res. 50 (2013) 34–40, https://doi.org/10.1016/J.CEMCONRES.2013.03.020.
[112] Z. Yang, W. Ren, R. Sharma, S. McDonald, M. Mostafavi, Y. Vertyagina, T.J. Marrow, In-situ X-ray computed tomography characterisation of 3D fracture evolution and image-based numerical homogenisation of concrete, Cem. Concr. Compos. 75 (2017) 74–83, https://doi.org/10.1016/J.CEMCONCOMP.2016.10.001.
[113] K. Wan, X. Xue, In situ compressive damage of cement paste characterized by lab source X-ray computer tomography, Mater. Charact. 82 (2013) 32–40, https://doi.org/10.1016/j.matchar.2013.05.004.
[114] S. Erdem, A.R. Dawson, N.H. Thom, Impact load-induced micro-structural damage and micro-structure associated mechanical response of concrete made with different surface roughness and porosity aggregates, Cem. Concr. Res. 42 (2012) 291–305, https://doi.org/10.1016/j.cemconres.2011.09.015.
[115] A. du Plessis, I. Yadroitsava, S.G. le Roux, I. Yadroitsev, J. Fieres, C. Reinhart, P. Rossouw, Prediction of mechanical performance of Ti6Al4V cast alloy based on microCT-based load simulation, J. Alloys Compd. (2017), https://doi.org/10.1016/j.jallcom.2017.06.320.
[116] E. Coleri, J.T. Harvey, K. Yang, J.M. Boone, Development of a micromechanical finite element model from computed tomography images for shear modulus simulation of asphalt mixtures, Constr. Build. Mater. 30 (2012) 783–793, https://doi.org/10.1016/J.CONBUILDMAT.2011.12.071.
[117] H. Wang, Z. Huang, L. Li, Z. You, Y. Chen, Three-dimensional modeling and simulation of asphalt concrete mixtures based on X-ray CT microstructure images, J. Traffic Transp. Eng. (English Ed.). 1 (2014) 55–61, https://doi.org/10.1016/S2095-7564(15)30089-1.
[118] E.N. Landis, J.E. Bolander, Explicit representation of physical processes in concrete fracture, J. Phys. D Appl. Phys. 42 (2009) 214002–214017, https://doi.org/10.1088/0022-3727/42/21/214002.
[119] Y. Huang, Z. Yang, W. Ren, G. Liu, C. Zhang, 3D meso-scale fracture modelling and validation of concrete based on in-situ X-ray Computed Tomography images using damage plasticity model, Int. J. Solids Struct. 67–68 (2015) 340–352, https://doi.org/10.1016/J.IJSOLSTR.2015.05.002.
[120] Ł. Skarżyński, M. Nitka, J. Tejchman, Modelling of concrete fracture at aggregate level using FEM and DEM based on X-ray μCT images of internal structure, Eng. Fract. Mech. 147 (2015) 13–35, https://doi.org/10.1016/J.ENGFRACMECH.2015.08.010.
[121] W. Trawiński, J. Bobiński, J. Tejchman, Two-dimensional simulations of concrete fracture at aggregate level with cohesive elements based on X-ray μCT images, Eng. Fract. Mech. 168 (2016) 204–226, https://doi.org/10.1016/J.ENGFRACMECH.2016.09.012.
[122] Ł. Skarżyński, J. Tejchman, Experimental investigations of fracture process in concrete by means of x-ray micro-computed tomography, Strain 52 (2016) 26–45, https://doi.org/10.1111/str.12168.
[123] W. Ren, Z. Yang, R. Sharma, C. Zhang, P.J. Withers, Two-dimensional X-ray CT image based meso-scale fracture modelling of concrete, Eng. Fract. Mech. 133 (2015) 24–39, https://doi.org/10.1016/J.ENGFRACMECH.2014.10.016.
[124] J. Gerber, K. Jenkins, Finite element modelling and damage quantification of chip seals, Road Mater. Pavement Des. 18 (2017) 350–361, https://doi.org/10.1080/14680629.2016.1213512.
[125] M.A.B. Promentilla, T. Sugiyama, T. Hitomi, N. Takeda, Quantification of tortuosity in hardened cement pastes using synchrotron-based X-ray computed microtomography, Cem. Concr. Res. 39 (2009) 548–557, https://doi.org/10.1016/J.CEMCONRES.2009.03.005.
[126] Y.-S. Wang, J.-G. Dai, X-ray computed tomography for pore-related characterization and simulation of cement mortar matrix, NDT E Int. 86 (2017) 28–35, https://doi.org/10.1016/J.NDTEINT.2016.11.005.